npj | Materials Degradation

www.nature.com/npjmatdeg

REVIEW ARTICLE OPEN

The development of β phase Mg–Li alloys for ultralight corrosion resistant applications

Taylor W. Cain [1]✉ and Joseph P. Labukas[1]

Magnesium alloys with high lithium concentrations possess a lightweight body centered cubic (BCC) matrix structure with densities in the range of 1.3–1.65 g/cm^3. These alloys have shown the ability to provide an excellent combination of strength, ductility, and corrosion resistance. Despite these great properties, the developmental history of Mg–Li alloys has observed widely varying degrees of interest but has regained momentum over the past decade. The intention of this review is to provide an overview of the mechanical properties and available corrosion data from inceptive BCC Mg–Li alloy reports to contemporary works with an emphasis on the chemical and microstructural aspects contributing to corrosion behavior. A discussion on the state of the art of the corrosion mechanism of BCC Mg–Li alloys is provided with an emphasis on hi fidelity characterization techniques that were not available to early researchers working on the Mg–Li system. In the current state, there remains a great potential for further improvement in the mechanical properties and corrosion resistance.

npj Materials Degradation (2020)4:17 ; https://doi.org/10.1038/s41529-020-0121-2

INTRODUCTION

Development of lightweight metals with high specific strength and improved plasticity remains of high priority to the automotive, aerospace, and defense industries where reducing mass is requisite to increasing fuel efficiency and reducing emissions[1,2]. Currently, magnesium–lithium (Mg–Li) base alloys present tremendous potential for ultralight structural metals as the low density of Li ($\rho = 0.53$ g/cm^3) can reduce the density of Mg alloys from 1.77–1.83 g/cm^3 to 1.3–1.65 g/cm^3. Magnesium–Lithium alloys are unique in that three different crystal structure configurations can result depending on the lithium concentration. The first structure is based on the α-Mg hexagonally close packed (HCP) unit cell which is stable to approximately 5.7 wt% Li. Second, a duplex α + β phase field exists between 5.7 wt% Li to ~10.3 wt% Li. Finally, the β-body centered cubic (BCC) solid solution is stable beyond 10.3 wt% or a Mg/Li ratio of less than 8.7 by mass. Of these base states, α-Mg alloys possess the highest strength and greatest work hardenability, α + β alloys possess moderate strengths, increased ductility and good work hardenability, and β-Li alloys possess the lowest strength, greatest ductility, and least work hardenability[3–5]. Thus, the β-BCC structure is of high interest as it has a greater number of slip planes available in comparison to the α-HCP structure, which enables improved formability and decreases in texture anisotropy[6–8]. Such properties make Li rich α + β and β alloys attractive materials for development in highly formable, lightweight applications.

Development of Mg–Li alloys has been of interest to the scientific community since as early as 1935 when a U.S. patent was granted for use of Mg–Li alloys as a sacrificial clad coating[9]. However, it was not until after World War II when interest in the bulk properties of Mg–Li alloys grew rapidly in the United States and former Soviet Union[3,4,10–22]. These early studies showed that average yield and tensile strengths above 300 MPa could be achieved. However, interest in the development of Mg–Li alloys declined as microstructural instability could not be controlled at temperatures below 100 °C leading to rapid overaging of alloys[3,12,14,18,19]. It was after this realization that most of the development of Mg–Li alloys in the United States focused on thermomechanical processing and weldability studies of alloys for commercial use. Of the alloys to come from this era, wrought LA141A-T7 (Mg-14Li-1.5Al) featuring a stabilized AlLi phase was the most popular and found use in military and aerospace applications while high alloyed, higher strength alloys such as LA136 (Mg-13Li-6Al) suffered from cast ingot segregation and poor weldability[23–25]. These issues, in addition to the inherent safety challenges of handling Li (see Supplemental Text) during alloy preparation, contributed to dwindling interest and research efforts after the 1970's. However, renewed interest in Mg–Li alloys over the last decade has been driven largely by advances in analytical tools developed within academic community, providing opportunities to advance the state of art for the BCC Mg–Li alloy system.

The synthesis, corrosion resistance, and surface treatment of some Mg–Li alloys has been reviewed recently in two manuscripts[26,27]. Wu et al.[26] provide an excellent review on the synthesis of Mg–Li alloys with an emphasis on electrochemical methods for alloying while the review by Sun et al.[26,27] provides an overview of corrosion behavior and surface treatments across all classes of Mg–Li alloys. However, the review by Sun et al. does not provide a thorough synopsis on the electrochemical aspects of BCC Mg–Li alloy corrosion. The review herein seeks to build upon these works by combining discussion of historical alloy development with intrinsic corrosion reports of BCC Mg–Li alloys while linking them to a contemporary understanding of the Mg corrosion mechanism. We provide first a brief summary on the strengthening behavior and microstructural aspects of BCC Mg–Li alloys as readers may not be familiar with the alloy systems that have been developed. This discussion provides a secondary benefit of alluding to the microstructures that may be present but were not discussed in the corrosion evaluations by early developmental works. This is followed by a review of the state of the art on the corrosion behavior of BCC Mg–Li alloys with an emphasis on describing the effect of alloying and associated microstructural aspects on the strengthening and corrosion resistance of BCC Mg–Li alloys. Finally, we will provide an outlook

[1]CCDC Army Research Lab, 6300 Rodman Rd, Aberdeen Proving Ground, MD 21005, USA. ✉email: taylor.w.cain2.civ@mail.mil

Published in partnership with CSCP and USTB

npj nature partner journals

on areas of need and suggestions for novel corrosion resistant alloy synthesis.

MICROSTRUCTURAL DEVELOPMENT AND THE PROBLEM OF INSTABILITY IN BCC MG–LI ALLOYS

Early developmental efforts in the 1940's and 1950's embarked on a vast endeavor to understand the strengthening effects and stability of alloying elements in Mg–Li alloys. Figure 1 shows a plot of yield strength vs. elongation to failure for Mg–Li alloys from these archival efforts as well as data from more recent works. We chose to use yield strength as this value represented the most common metric in the literature for a basis of comparison. It is readily apparent that the property range of BCC Mg–Li alloys follows the characteristic inverse relationship expected between yield strength and elongation of metals. It should be noted that not all of the values reported in this plot are representative of the stable alloy but are values after certain heat treatments. Many of the alloys reported exhibit microstructural instability and room temperature loss of strength with time. However, Fig. 1 highlights alloys with reasonably stable microstructures of which garnered industrial interest—their compositions are provided in Table 1. Many of these alloys contain common Mg alloying additions such as Al and Zn. Indeed, the seminal report on Mg–Li alloy development by Jackson et al.[3] comprehensively established Al, Zn, Cd, and Ag additions as providing the greatest strengthening effects in the β crystal structure. This is shown in Fig. 2 where the relative strengthening effects of ternary alloying additions on extruded alloys with an Mg/Li ratio of 8.1 is given. It was reported by Jackson and others[3,5,12,14,18,28,29] that high hardness of Al, Zn, Ag, and Cd ternary alloys can be achieved after hot working and/or water quenching from high temperatures but these alloys were unstable at temperatures under 100 °C. Such microstructural instability led to softening at aging times <48 h. These early studies attributed the age hardening of alloys containing Al, Zn, Ag, and Cd to the coherency of an intragranular, cubic, metastable transition θ-phase whose composition was approximated to be $MgLi_2X$, where X = (Al, Zn, Cd), based on X-ray analysis. In the case of Mg–Li–Ag, Raynor and Kench proposed that the transition phase chemistry did not follow $MgLi_2X$ but instead was a stable structural variation of BCC Mg–Li–Ag phase with a high concentration of Li[30]. In general, the rapid overageing of these alloys was attributed to a loss in coherency due to increasing mismatch in lattice constants between the β-matrix and θ-phase over time and decomposition of θ to equilibrium phases such as AlLi and ZnLi. Additional loss in strength was attributed to coarsening of θ-phase along grain boundaries though this effect was found to be less for Ag than Al, Zn, and Cd, respectively[18,19,31]. In contrast to these early studies, a recent study of a Mg–Li–Al based alloy by Tang et al. using a modern suite of characterization methods have shown that the identity of the transition phase is a semi-coherent, cubic DO_3-$MgAl_3$ nanophase as shown in Fig. 3. However, it is not clear if this structure also forms in the Zn, Ag, and Cd containing alloys[32]. Regardless of the identity of the transition phase, decomposition of these strengthening precipitates to equilibrium phases such as AlLi and ZnLi leads to loss of strength over time at low temperatures.

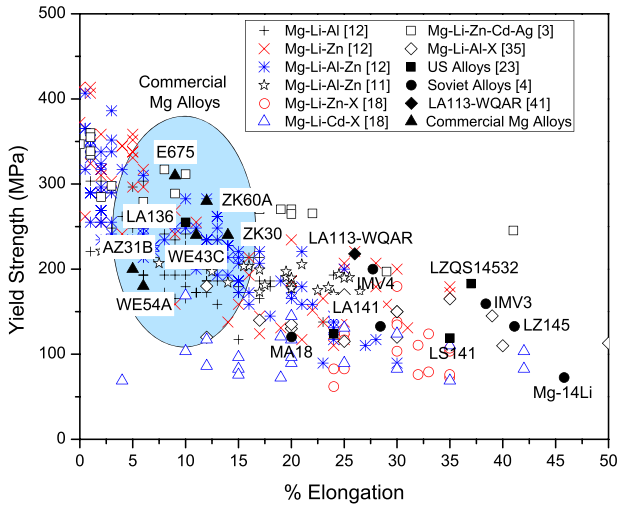

Fig. 1 The Property Space of Mg-Li based Alloys. A plot of percent elongation to failure vs yield strength. Prominent Mg–Li alloys are noted by enclosed black squares and compared with commercial Mg alloys enclosed circles. Data compiled from the following works and technical sheets from Magnesium Elektron Ltd.[3,4,11,12,18,36,41].

A number of observations are evident on the strengthening and stability of the transition phase in β Mg-Li alloys based on early studies. First, elements with large super saturated solubility in the β phase such as Al, Zn, Ag, and Cd are those which provide the greatest age hardening response[3,12,14,18,28]. This assertion falls under the premise that highly soluble elements provide improved coherency between the β-matrix and transition phases leading to impeded dislocation motion. Furthermore, greater elemental super saturated solubility generally increases the maximum volume fraction of a strengthening precipitate. In contrast, small additives of insoluble elements provided no benefit to hardening and stability of Mg–Li–Al[14] and some benefit to Mg–Li alloys containing Zn, Cd, and Ag[33]. This was attributed to the insoluble elements not affecting the magnitude of the crystal lattice discrepancy such that crystallographic matching between the matrix and precipitates becomes favorable for maintaining coherency. In such cases where incoherent phases form, dislocation motion is easily accommodated by Orowan looping leading to low strength and work hardening responses. The general solubility of elements in β-solid solution is shown in Table 2 which highlights that little is known about the solubility and hardening response of rare earth (RE) elements in β-phase.

Research was performed in the former Soviet Union on the hardening response of ternary additions of Ce, La, Nd, and Y in concentrations up to 3–5 wt%. These studies revealed an increase in strength of about 10–15% from the binary Mg–Li alloy, which is far less than that discovered for Al, Zn, Ag, and Cd additions. While these alloys did not suffer the degree of softening as Mg-Li alloyed with Al and Zn, the weak strengthening did not warrant use of RE's as a primary alloying element[4,28]. The lack of a hardening response for these ternary alloys was attributed to the low terminal solubility of these RE elements in β-solid solution (Table 2) and formation of eutectic structures along grain boundaries. The strengthening effect of the remaining RE metals (Z > 60) in the β-solid solution has not yet been determined. It stands to reason that these elements, which possess high super saturated solubility in α-Mg[34], may also have high super saturated solubility in the β-solid solution as many of the highly soluble elements in the β-solid solution are also highly soluble in α-Mg[35]. Such high super saturated solubility may lead to an excellent aging response but further experimental investigation is required.

Recently, alloys with combinations of Al or Zn alloying additions along with Zr and RE elements have been investigated[36–45]. These alloys have been reported to introduce additional microstructural complexity in the form of Al_xRE_y intermetallic phases, which can provide particle strengthening and the possibility of long-period stacking order (LPSO) phases. For example, Chakravorty found reasonably good mechanical property retention in the stabilized condition for Mg-11Li-1.5Al-0.14Zr[36] but the strength was further improved by Xu et al.[41] by increasing the Al concentration and adding Y (Mg-10.95Li-3.29Al-0.19Zr-0.59Y, noted as LA113-WQAR in Fig. 1). Particle dispersed strengthening by Al_2Y was found in this alloy and others[37,40,42] have been reported to improve

Table 1. Nominal composition in wt% of successful alloys developed for commercial application prior to 1972[4,23].

Alloy designation	Origin	Li	Al	Zn	Cd	Mn	Other	Density (g/cm^3)	Mg/Li ratio
Wrought									
LA141A	USA	13–15	0.75–1.3	–	–	0.15	–	1.35	5.6–6.6
LA136	USA	13–15	5–7	–	–	0.1–0.3	–	1.64	5.2–6.3
MA18	USSR	10–11.5	0.5–1	2.0–2.5	–	0.1–0.4	0.15–0.35 Ce	1.48	7.3–8.7
Cast									
LS141	USA	14	–		–	–	0.5 Si	1.33	6.1
LZQ1453	USA	14	–	5	–	–	3 Ag	1.48	5.6
LZQS14532	USA	14	–	5	–	–	3 Ag, 2 Si	1.51	5.4
IMV3	USSR	14	–	5	–	–	–	1.38	5.8
IMV4	USSR	14	1	5	–	–	–	1.39	5.7

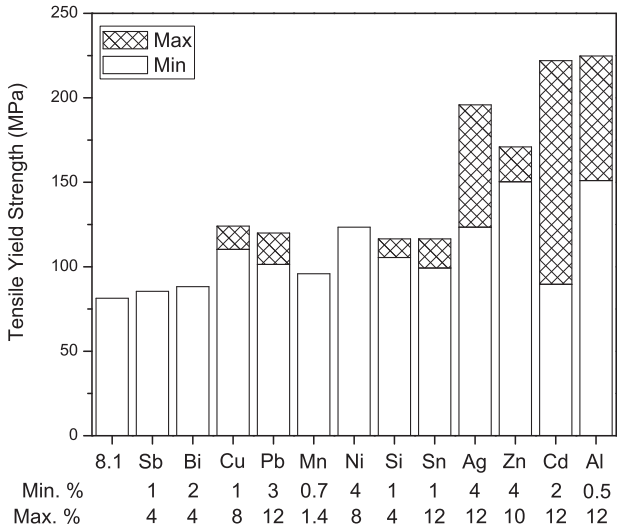

Fig. 2 The relative strengthening effect of ternary element additions to β Mg-Li Alloys. The effect of ternary elements on the tensile yield strength for as extruded alloys with an Mg/Li mass ratio of 8.1. The minimum and maximum alloy element concentrations are given. Reproduced from Jackson et al.[3].

microstructural refinement leading to favorable combinations in strength and ductility. The addition of Nd[38] to BCC Mg–Li–Al alloys produced similar grain refinement and improvement in mechanical properties while addition of Ce[43] and La[44] provided little strengthening effect. To date, little is known about the formation and stability of long period stacking order (LPSO) phases in BCC Mg–Li alloys and a recent attempt to form such a phase via Mg-Li-Zn-Y-Er alloys was not successful[45]. This result likely is due to unfavorable formation of stacking faults in BCC metals which is a component to LPSO phase formation. However, LPSO phases have been formed in α + β Mg–Li alloys with a positive effect on strength and ductility[39].

CORROSION MECHANISM AND SURFACE FILM STRUCTURE

Magnesium corrosion is described by the following electrochemical reactions:

$$\text{Anodic}: Mg \rightarrow Mg^{2+} + 2e^- \quad E^o = -2.37V_{SHE} \tag{1}$$

$$\text{Cathodic}: 2H_2O + 2e^- \rightarrow H_2 + 2OH^- \quad E_{pH,7} = -0.414V_{SHE} \tag{2}$$

$$\text{Overall Reaction}: Mg + 2H_2O \rightarrow Mg(OH)_2 + H_2 \tag{3}$$

Upon full-immersion in aqueous electrolytes, the oxidation of Mg and reduction of H_2O occur simultaneously at the Mg-water interface resulting in a layered surface oxide comprising MgO and $Mg(OH)_2$[46,47]. This discontinuous mixed oxide/hydroxide film provides minimal protection against further corrosion due to the slight aqueous solubility of the oxide/hydroxide at pH < 11, a mismatch in lattice parameters at the oxide-metal interface such that the Pilling-Bedworth ratio is less than unity, and susceptibility of film breakdown by detrimental anions such as chlorides and sulfates[48]. Under atmospheric conditions, the corrosion behavior of Mg and Mg alloys is much different due to the complex chemistry and morphology that develops within the surface oxide film. A recent review highlights the need for a thorough understanding of the atmospheric corrosion of Mg alloys and provides an in-depth overview on corrosion mechanisms under thin film conditions[49]. To date, there have been no mechanistic studies on the atmospheric corrosion of BCC Mg–Li alloys to date and the role of CO_2, SO_2, N_2, and O_2 on the corrosion behavior is unknown. However, the aqueous corrosion rate of Mg alloys is generally controlled by the constant evolution of hydrogen from the Mg surface.

For BCC Mg-Li alloys with >30 at% Li, additional anodic reactions with Li are expected:

$$\text{Anodic}: Li \rightarrow Li^+ + e^- \quad E^o = -3.04V_{SHE} \tag{4}$$

$$\text{Overall Reaction}: 2Li + H_2O = 2LiOH + H_2 \tag{5}$$

The surface film that forms on BCC Mg–Li alloys is known to provide improved passivity in aqueous electrolytes in comparison to the α and α + β structures[50]. Recently, Al, Zr, and Y additions to BCC Mg-Li alloys have resulted in corrosion rates lower than any known commercial Mg alloy[41]. Using X-ray photoelectron spectroscopy (XPS) and X-ray diffraction (XRD), a Li_2CO_3-containing surface layer was revealed and it was hypothesized to provide barrier properties that contribute to the low corrosion rates in aqueous full-immersion conditions[41,50,51]. For Mg alloys that do not contain Li, the role of CO_2 and the formation of Mg hydroxycarbonates have a beneficial effect on corrosion by blocking anodic and cathodic sites as well as lowering pH and local solution conductivity in thin film (atmospheric) corrosion[41,51]. The corrosion mechanism in BCC Mg-Li system varies from this as magnesium carbonates have not been detected by XPS or XRD. Recent calculation of chemical stability diagrams for Mg and Li carbonates in a full immersion condition suggest that the carbonate species is only stable at high aqueous Li concentrations and pH >10, and the K_{sp} for $LiCO_3$ is on the order of ~10^{-2} whereas $Mg(OH)_2$ and

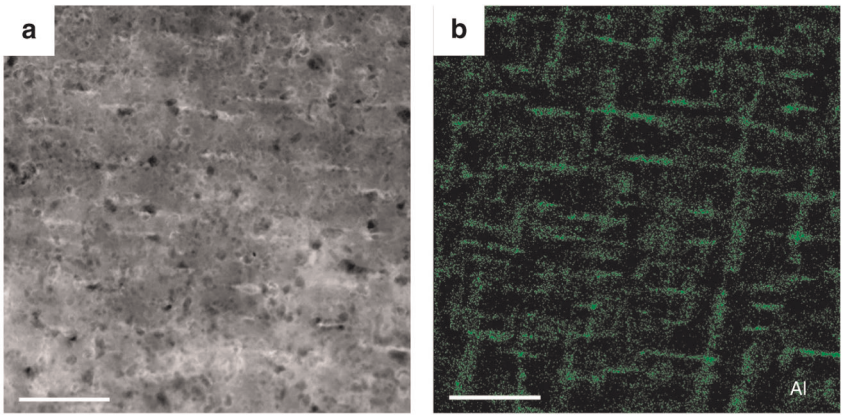

Fig. 3 The Nanoscale Microstructure of an Mg-Li-Al Alloy. a Scanning transmission electron image of LA113-WQAR alloy and **b** Al elemental map, both with 200 nm scale bar[32] (adapted from ref. [32] under Creative Commons Attribution 4.0 International License).

Table 2. Relative terminal solubility of elements in β Mg–Li[3,4].

Terminal solubility	Elements
Large (>1 wt%)	Al, Ag, Cd, Hg, In, Tl, Zn
Some (<c.a. 1 wt%)	Ba, Bi, Ca, Ce, Co, Cu, Ge, La, Nd, Ni, Pb, Sb, Si, Sn, Sr, Y
Insoluble (<0.1 wt%)	B, Be, Cb, Cr, Fe, K, Mn, Mo, Th, Ti, U, V, W, Zr

$MgCO_3$ are ~10^{-12} and ~10^{-6}, respectively[41,51–54]. However, such a condition may be met under thin aqueous film as in atmospheric corrosion or with air.

The chemical composition and structure of the surface film formed upon immersion in NaCl (aq) has been performed using several surface sensitive techniques including grazing incidence X-ray diffraction (GIXRD), Raman spectroscopy, XPS, electron energy loss spectroscopy (EELS), selected area electron diffraction (SAED), and scanning transmission electron microscopy (STEM). The combined information of these techniques have revealed a complex film that comprises many possible modes of protection against corrosion. The data suggest an outermost layer that is rich in Li (Fig. 4) causing phase transformation and formation of an HCP Mg-Li crystal structure within the Li depleted matrix[51,55,56]. This evidence is consistent with non-stoichiometric Li dissolution where excess Li is observed during immersion and Li_2CO_3 formation at a surface dried in air. The repassivation[57] of the surface films formed on the Mg–Li(-Al, Zr, Y) alloy system was found during scratch testing and can be attributed to the complicated interplay between several components that have been identified most recently by Yan et al.[56] Importantly, in situ Raman analysis in this work revealed the dissolution of Li_2CO_3 with immersion time suggesting that Li_2CO_3 is air formed and not responsible for repassivation of the dissolving Mg–Li(–Al–Zr–Y) surface. In addition, Li–Al layered double hydroxides (LDH) and $Mg(OH)_2$ were found at Al_2Y particles in actively corroding areas as shown schematically in Fig. 5. This research suggested that air-formed Li_2CO_3 is not protective under full immersion in contrast to the hypothesis of earlier studies. The authors hypothesize a Li cation-doped MgO film with Pilling-Bedworth ratios >1 at alloy Li concentrations >15 at% is able to provide theoretical passivity. As such, the 100 nm thick Li-doped oxide exhibited improved stability and resistance to decomposition which rationalizes the excellent corrosion resistance of these alloys[56].

THE EFFECT OF MAJOR ALLOYING ELEMENTS ON THE CORROSION OF BCC MG–LI ALLOYS

Profile of strength and corrosion resistance

Assessing the effect of major alloying elements on the corrosion resistance of Mg–Li alloys is difficult for a number of reasons. The primary reason for this is that the largest number of alloy compositions was evaluated before 1967 where there is a paucity of available microstructural information (i.e., phase fraction, size, distribution, morphology) with which to correlate trends in the measured corrosion resistance[11,23]. Furthermore, corrosion testing in this era predated use of the potentiostat for electrochemical evaluation and typically involved alternate immersion testing in 3% NaCl at 35 °C and atmospheric testing at 100% humidity at 35 °C; as was performed by the Battelle Memorial Institute where thousands of individual heats of α + β and β alloys were synthesized[3,11]. These types of experiments are not directly comparable to results obtained from the now commonly performed full immersion testing and accelerated atmospheric testing in accordance with ASTM B117. However, it is still relevant herein to describe the property space with respect to selected mechanical and corrosion properties. Figure 6 shows a plot of the corrosion rate from alternate immersion testing of Mg-Li-Zn-Cd-Ag[3] and Mg-Li-Al–Zn[11] versus yield strength. Also included in this figure are data for alloys developed by the former Soviet Union[22] and the 'stainless' Mg alloy LA113 (Mg-Li-Al-Zr-Y)[41]. It should be noted that the corrosion data from these reports cannot be directly compared with each other on this plot except for the works of Frost et al.[11] and Jackson et al.[3] but a relevant baseline was collected in the other studies by which the corrosion performance can be compared. With respect to works by Jackson et al.[3] and Frost et al.[11], the corrosion rates can be compared with those of AZ31 and M1A whose values were determined using the same alternate immersion testing method. It is readily apparent that all alloy compositions from these studies have corrosion rates more than 4× greater than that of AZ31. With respect to efforts in the former Soviet Union, Drits et al. reported low mass loss rates for stabilized, industrial alloys MA18, IMV3, and IMV4 in comparison to the LA141 which has been reported to have a similar corrosion rate to M1A and AZ31 in humidity testing[22]. The data from these three studies indicate that a combination of excellent mechanical properties and corrosion resistance was not made. However, the alloy developed by Xu et al.[41] was able to achieve a high yield strength on par with commercial Mg alloys (Fig. 1) and maintain corrosion mass loss rates more than one order of magnitude less than that of pure Mg. As such, this alloy represents the most promising combination of mechanical

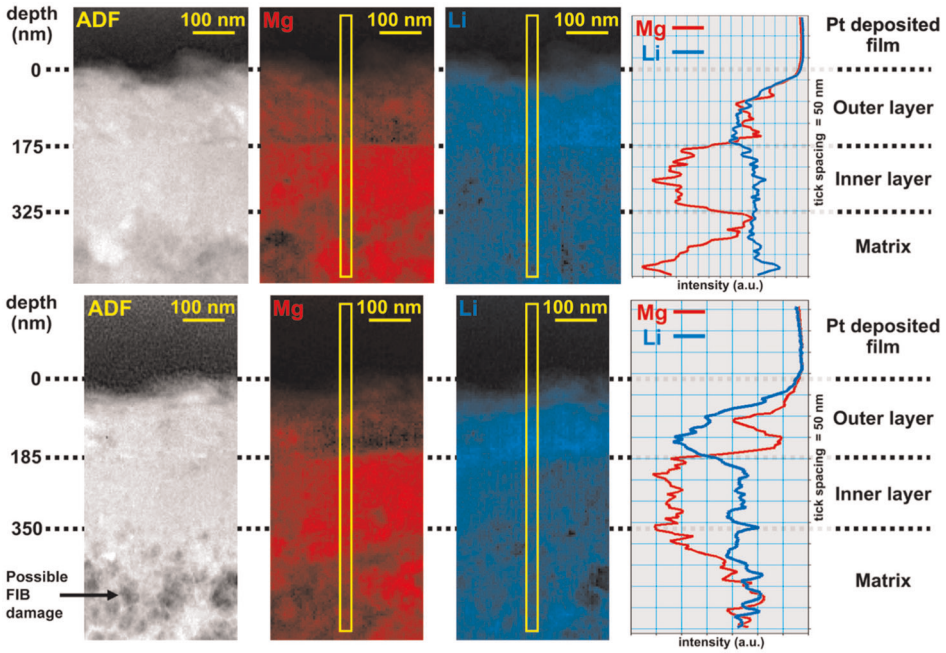

Fig. 4 Corrosion Film Cross Section of an Mg-Li-Al Alloy. Annular dark-field images and corresponding EELS map for two TEM specimens of LA113 after 24 immersion in 0.1 M NaCl and subsequent exposure to air for 7 days. The yellow boxes indicate the loci of where the intensity profiles were taken[55] (reprinted with permission from ref. [55], copyright Elsevier 2019).

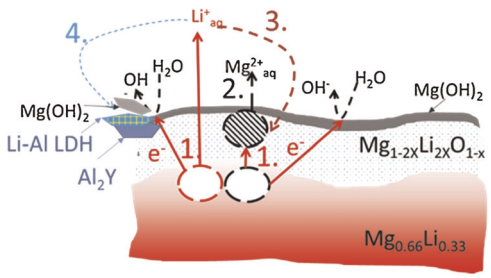

Fig. 5 A schematic representation of corrosion film structure on the LA113 alloy surface. A schematic illustration of the corrosion film structure of LA113 as shown by Yan et al.[56] (reproduced with permission from ref. [56], copyright Elsevier 2020).

properties and corrosion resistance of any BCC Mg–Li alloy to date.

The effect of Al and Zn on corrosion of BCC Mg–Li alloys

Frost et al. evaluated the effect of Al in ternary Mg–Li–Al alloys at Mg/Li ratios of 8.1 and 6 by mass[11]. They found that corrosion resistance of Mg/Li = 6 increased monotonically for Al additions up to 3.5 wt% while there was no trend for Mg/Li = 8.1. Furthermore, the corrosion rates measured for Mg/Li = 6 were less than those of Mg/Li = 8.1 suggesting that increasing the Li concentration increases the corrosion resistance. In agreement with these findings, Matsuzawa et al.[58] measured a monotonic increase in corrosion resistance with increasing Al concentration for warm rolled sheets during atmospheric corrosion of Mg-13Li-*x*Al ($x = 1, 3, 5$). More recent studies evaluating the effect of Al on the corrosion rates of BCC Mg–Li alloys provide data on the effects of microstructure. Morishige et al.[59] found that the corrosion rate decreased with increasing Al to a measured composition of 3.37 wt% Al before rising rapidly with further Al addition for cast and homogenized Mg-14Li-*x*Al ($x = 1, 2, 3, 5$)

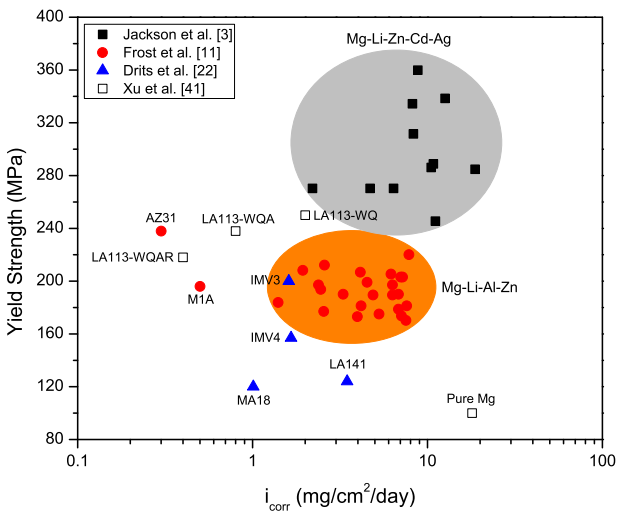

Fig. 6 The Property Space of Strength and Corrosion Resistance. The corrosion rate vs. yield strength for BCC Mg–Li alloys with available data. The data for Jackson et al.[3] and Frost et al.[11] was measured after 8 day alternate immersion in 3% NaCl. Drits et al.[22] reported corrosion rate after full immersion in 3% NaCl. Xu et al.[41] measured mass loss after a 24-h immersion in 0.1 M NaCl.

alloys in 5 wt% NaCl saturated with $Mg(OH)_2$. Potentiodynamic polarization experiments in this investigation revealed pseudo-passive behavior for Al = 2 and 3 wt%. In addition, Morishige et al.[59] synthesized bulk AlLi intermetallic phase and evaluated the effect of volume fraction of AlLi phase on the corrosion rate. The corrosion potential of AlLi phase was found to be about 300–400 mV more negative than that of the alloys (-2 $V_{Ag/AgCl}$) which contributed to increased corrosion rates with increasing AlLi fraction as would be expected for a micro-galvanic couple. The AlLi phase was found largely along grain boundaries, which

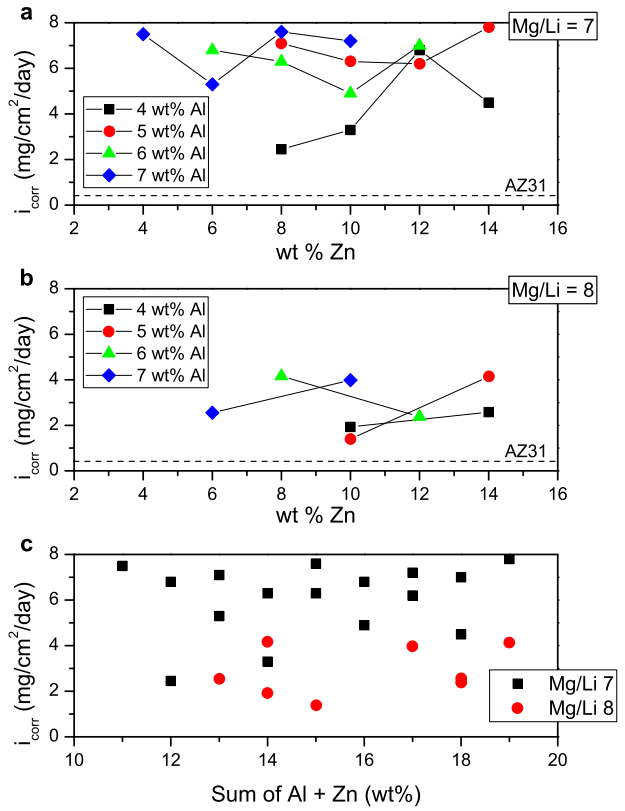

Fig. 7 The effect of Al and Zn on the corrosion of Mg-Li alloys. a The corrosion rates of 7Mg/Li–Al–Zn alloys, **b** Mg/Li–Al–Zn alloys and **c** the effect of the sum of Al and Zn on corrosion of 7Mg/Li–Al–Zn and 8Mg/Li–Al–Zn. Data from Frost et al.[11].

appeared to constrain filiform-like corrosion to grain specific corrosion with an increasing fraction of AlLi. In a different study, Li et al.[60] observed AlLi phase along grain boundaries in an as cast Mg-15.9Li-6.2Al alloy while a uniform distribution of short rod like precipitates of $MgLiAl_2$ were found within grains. The even distribution of $MgLiAl_2$ and near continuous formation of AlLi along the grain boundaries promoted uniform corrosion attack and was hypothesized to act as a corrosion barrier similarly to the barrier effect of $Mg_{17}Al_{12}$ observed in AZ91[61]. Although the $Mg_{17}Al_{12}$ intermetallic is beneficial for corrosion of Mg alloys in certain morphologies, most other intermetallic species can be detrimental to the corrosion rate.

Frost et al.[11] measured the effect of Zn on the corrosion of 8.1Mg/Li and found it be much worse than that of Mg–Li–Al. These authors also found that the effects of Mg–Li–Al–Zn alloys provided varying results for large alloying additions between 4–7 wt% Al and 4–14 wt% Zn as shown in Fig. 7. Figure 7a, b show the change in corrosion rate as a function of Zn concentration for different levels of Al and two different concentrations of Li. It is evident from these plots that no distinctive trends can be made for increasing Zn concentration. However, the corrosion rate does seem to rise with increasing Al for a given concentration of Zn, but the overall trend is weak. The results of this study also show that corrosion rate decreases with decreasing Li (Fig. 7c) which is in contrast to other results in this study, as discussed above. A contributing factor to this discrepancy may be due to undetermined microstructural variation in secondary Al, Zn containing phase size, fraction, distribution, morphology, and chemistry. The lowest corrosion rate measured by Frost et al. was a mass loss of 1.4 mg/cm^2/day after 192 h alternate immersion in 3% NaCl for 8Mg/Li-10Zn-5Al which was 3.5× greater than that measured for 'hard rolled' AZ31. Frost et al. acknowledged that scatter in the results is likely sensitive to unidentified segregation, impurities, and precipitates. In another work, Kazakov et al.[62] performed a brief study on the effect of Zn additions to Mg–14Li–1Al and found that the corrosion rate decreased with additions up to 2 wt % Zn before increasing.

Corrosion behavior of RE element containing BCC Mg–Li alloys

The corrosion resistance of a small number of RE containing alloys has been studied and the role of RE elements on corrosion resistance of Mg–Li alloys has not been comprehensively established[41,51,56,57,62–64]. Most literature reports on RE element additions to Mg–Li alloys also use Al as an alloying element so it is likely that the RE elements are incorporated in Al_xRE_y particles as described above. It has not yet been determined if these particles are anodic or cathodic with respect to the β Mg–Li alloy matrix. However, they do not appear to play a dominant role in corrosion of alloys containing less than 1 wt% of RE elements, as indicated with LA113 in the works of Xu et al. and Yan and co-workers (*vide supra*)[41,51,56,57]. In other works, Kazakov et al. compared the corrosion rates of stabilized MA18 (Mg-11Li-0.9Al-2.2Zn-0.1Mn-0.2Ce) to VMD5-1 (Mg-13.5Li-0.8Al-2.4Zn-0.11Mn-0.24Ce) and measured slightly greater corrosion resistance in MA18 which possesses lower Li and Ce concentrations[62]. Meanwhile, recent work by Zhang et al.[63] tested an Mg-15Li-5Al-0.5RE alloy in varying concentrations of NaCl and pH. The authors did not specify the identity of the RE element but found that the corrosion resistance decreased with increasing Cl^- and increased with increasing pH. No microstructural or surface characterization was presented but electrochemical impedance spectroscopy (EIS) revealed the presence of high and low frequency capacitive loops where a low frequency capacitive loop is commonly attributed to a diffusional process due to the presence of a protective surface film. An additional study by Gao et al.[64] on Mg-11Li-3Al-0.5RE revealed similar trends in Cl^- activity and pH with pseudo passive behavior. However, 24-h immersion testing in 0.5 M NaCl (pH = 12) revealed a number of dark corrosion product in localized pits several millimeters in diameter.

Corrosion behavior of other Mg–Li alloys

Jackson and co-workers[3], compared the mass loss after alternate immersion experiments in 3% NaCl solution of Mg–Li–Zn–Cd–Ag alloys with Mg/Li mass ratios of 6.0, 7.0, and 8.1, AZ31, and M1A as previously discussed. Despite their high strengths, these alloys did not give adequate corrosion resistance as shown in Fig. 6. It can be noted that the lowest corrosion rates were generally observed for alloys with Mg/Li ratios of 7 or 8. Furthermore, the authors noted a trend of increasing corrosion rate with an increase in the sum of Ag and Zn content but further investigation is required to understand the individual role of Zn, Ag, and Cd on corrosion rate.

The effect of impurities on corrosion of BCC Mg–Li alloys

The effect of impurities such as Fe, Cu, and Ni on the corrosion behavior of Mg has long been known since the seminal works of Boyer as well as Hanawalt et al.[65–67]. The detrimental effect of these impurities is also applicable to Mg-Li alloys as well as additional elements such Na, K, and P—common impurities in Li metal or inclusions from the use of salt fluxes during melting. As with conventional Mg alloys, Mn was found to ameliorate the corrosion resistance of LA142, in concentrations greater than 0.1 wt%, due to its ability to scavenge Fe from the melt[3,21]. The impurity threshold for Na has been the most studied impurity and early research efforts established the detrimental effect on ductility owing to the propensity of Na to migrate to and precipitate on grain boundaries[12,68]. The specific value for a

tolerance limit was much debated before being determined. Frost et al.[13] suggested an Na tolerance limit of 0.01% to achieve full ductility but did not report Na effects on corrosion resistance. It was later noted by Payne and Enyon[68] that this tolerance limit is likely lower and dependent on thermal history as significant corrosion occurred for alloys with an Na content greater than 0.002%, including exfoliation of the oxide/corrosion layers after 6–7 years exposure to lab air. Likewise, potassium and phosphorous inclusions from flux materials have similar threshold values and embrittlement behavior, critical to stress corrosion resistance[22].

Stress corrosion behavior of BCC Mg–Li alloys

Very few studies have been performed on the stress corrosion fatigue and cracking behavior of Mg–Li alloys[12,14,69]. Frost et al.[14] found that Mg–Li–Al–(Sn, Zn) α + β alloys possessed similar stress corrosion resistance as AZ31A under tensile loads of 30–75% of the yield strength, while Busk et al.[12] noted poor stress corrosion sensitivity of Mg-Li-Al-Zn alloys with a failure threshold load of <69 MPa using a spring load tension test in "rural atmosphere". Kiszka performed a more thorough evaluation of β–Mg–14Li–x based alloys with x = Al, Zn, Ag, and Si[69]. Testing was performed at the yield strength and 70% of the ultimate tensile strength in an environment of 85 to 100 % humidity with a temperature between 26.7–32.2 °C for 25 days. The results over a variety of heat treatments indicated that Al-containing alloys were susceptible to stress corrosion failure in the unstable state and failure occurred along grain boundaries. However, the stabilized state of Mg–14Li–xAl alloys after annealing at 150 °C for 48 h did not fail; Zn, Ag, and Si containing alloys sans Al did not fail in any of the heat-treated conditions in the 25 day test period. In another study, Kazakov et al.[62] compared the stress corrosion resistance of LA141 to MA18 and found superior stress corrosion resistance with M18 owing in part to its lower intrinsic corrosion rate.

The negative difference effect of BCC Mg–Li alloys

The anodic polarization of Mg alloys is unique in that increasing the anodic overpotential results in an increase in the rate of hydrogen evolution reaction, which is counter to conventional electrochemical theory. This observation has been widely termed the negative difference effect (NDE) or anodic hydrogen evolution and theories for its origin has been reviewed in detail elsewhere[49]. Briefly, theories for its manifestation have centered around the oxidation of univalent Mg[70–72], enhanced catalytic activity of corrosion products and noble impurity enrichment/deposition[73–77], Mg-hydride[78,79], and non-Faradaic release[80,81]. To date, only one study has examined the susceptibility of Mg–Li alloys to the NDE[82]. The results of this study revealed that NDE was indeed present for LA113 in 0.1 M NaCl and the anodic hydrogen evolution rates were very similar to that of pure Mg. This is an important finding as ~30% of the atoms in this alloy are Li and if the NDE were a result of the oxidation of univalent Mg in solution, then the anodic hydrogen evolution rate for LA113 would be much lower than that of pure Mg for a given applied anodic current density. The individual oxidation rates of Mg and Li were not measured in this study but atomic emission sepectroelectrochemistry (AESEC) results have shown Li oxidation is significant during dissolution of Mg–Li alloys[53,56,57]. Overall, the NDE is not an important factor in the intrinsic corrosion resistance of Mg alloys but it does play a role in the performance of Mg as a sacrificial alloy. It has been found recently that Mg alloys which exhibit a lower NDE as well as decreased cathodic kinetics have improved performance as sacrificial anodes for Mg alloys[83,84]. As Mg–Li alloys have been evaluated for use in sacrificial cladding[3,9], Mg–Li alloys which are less susceptible to the NDE are likely to provide lasting sacrificial protection. This same logic would also hold true for potential use of Mg–Li alloys as Mg-air batteries where the NDE limits the amount of anodic charge that can be transmitted through the circuit leading to poor efficiencies.

The anodically enhanced cathodic activation of BCC Mg–Li alloys

The anodically enhanced cathodic activation of Mg alloys has become of increasing interest in the past few years and is characterized by an increase in cathodic current density with increasing dissolution and corrosion product coverage[75,85–89]. While this observation has been linked to the NDE, it can be regarded as a separate effect important to improving the intrinsic corrosion resistance of Mg alloys. As the corrosion of Mg is cathodically controlled, methods to reduce the intrinsic cathodic reaction rate and anodically induced enhancement of the cathodic reaction rate with exposure time will lead to a longer life cycle and lower maintenance costs. As noted in the previous section, enhanced cathodic activity has been measured and modeled for $Mg(OH)_2$ covered surfaces[73,78,90,91] but the passivity and identity of corrosion films, not just Mg oxides/hydroxides, has been shown to play a role[92–94]. Passive films provide barrier protection to reduce ion migration through the film to the metal surface, act as an insulator and thus reduce the cathodic activity of the metal surface. It is likely that the identity of major alloying elements and elemental enrichment plays a dominant role in enhanced cathodic reaction as common elements and transition metals impurities possess higher exchange current densities for HER than Mg[74,88,95–100]. Recently, cathodic poisons such as As, Ge, and Bi have been shown to be effective to reduce the cathodic kinetics and resist anodically enhanced cathodic kinetics when alloyed with pure Mg[101–108] and may be promising for use in Mg–Li alloys. One recent study has demonstrated successful use of Ge as a cathodic poison for Mg–11Li binary alloys but additional work needs to be performed on the viability of cathodic poisons in Mg–Li alloys of industrial interest[109].

SUMMARY AND OUTLOOK

This review has presented an overview of the corrosion behavior of BCC Mg–Li alloys along with a discussion of the effects of alloying on mechanical properties and microstructure. It is apparent that while the largest research efforts on alloy development occurred more than 40 years ago, alloy development can benefit from modern characterization methods providing chemical and morphological details on the nanoscale. Use of techniques such as TEM and atom probe tomography should bring new insights toward development of stable high strength alloys, particularly alloys of the Mg–Li–Al family which have shown the greatest strengthening effect. Furthermore, there is a need to establish the strengthening effects of RE elements on with atomic number greater than 60.

While high strength and enhanced mechanical properties have traditionally driven alloy development, the intrinsic corrosion behavior cannot be ignored, especially for Mg–Li alloy systems where high corrosion rates have been observed. To date, very few Mg–Li alloys have been optimized for their mechanical and corrosion behaviors and there is much to learn about the Mg–Li corrosion mechanisms that will result from further alloy development and thermomechanical processing. There is also a paucity of electrochemical, surface, and microstructural data, which is necessary to correlate and explain corrosion behavior in these systems. Understanding of the corrosion behavior of novel and established BCC Mg–Li alloys stands to benefit greatly from the use of modern electrochemical methods and in situ techniques. Additionally, an understanding of the corrosion mechanisms of Mg-Li alloys in application relative environments is a necessary component of further development. This is particularly the case for atmospheric corrosion or thin aqueous films where the effect of

temperature fluctuations, CO_2, SO_2, N_2, and O_2 gases on corrosion behavior has not been evaluated for BCC Mg–Li alloys. Finally, micro alloying of cathodic poisons such as Sn and Ge represent great opportunity for improving the corrosion resistance of Mg–Li alloys.

DATA AVAILABILITY

The datasets generated during and/or analyzed during the current study are available from the corresponding author on reasonable request.

Received: 27 February 2020; Accepted: 8 May 2020;
Published online: 12 June 2020

REFERENCES

1. Brady, M. P., Joost, W. J. & David Warren, C. Insights from a recent meeting: current status and future directions in magnesium corrosion research. *Corrosion* **73**, 452–462 (2017).
2. Abbott, T. B. Magnesium: industrial and research developments over the last 15 years. *Corrosion* **71**, 120–127 (2015).
3. Jackson, J. H., Frost, P. D., Loonam, A. C., Eastwood, L. W. & Lorig, C. H. Magnesium-lithium base alloys—preparation, fabrication, and general characteristics. *JOM* **1**, 149–168 (1949).
4. Drits, M. Y., Sviderskaya, Z. A., Yelkin, F. M. & Trokhova, V. F. *Superlight Structural Alloys*. [in Russian] (Nauka, Moscow, 1972).
5. Kamado, S. & Kojima, Y. Deformability and strengthening of superlight Mg-Li alloys. *Metall. Sci. Technol.* **16**, 45–54 (1998).
6. Takuda, H., Matsusaka, H., Kikuchi, S. & Kubota, K. Tensile properties of a few Mg-Li-Zn alloy thin sheets. *J. Mater. Sci.* **37**, 51–57 (2002).
7. Shen, G. J. & Duggan, B. J. Texture development in a cold-rolled and annealed body-centered-cubic Mg-Li alloy. *Metall. Mater. Trans. A* **38**, 2593–2601 (2007).
8. Becerra, A. & Pekguleryuz, M. Effects of lithium, indium, and zinc on the lattice parameters of magnesium. *J. Mater. Res.* **23**, 3379–3386 (2011).
9. Brown, R. H. & Willey, L. A., Magnesium Duplex Metal. United States patent 2,011,613 (1935).
10. Hume-Rothery, W., Raynor, G. V. & Butchers, E. Equilibrium relations and some properites of magnesium-lithium and magnesium-silver-lithium alloys. *J. Inst. Met.* **71**, 589–601 (1945).
11. Frost, P. D., Whittenburg, R. V., Kura, J. G. & Eastwood, L. W. The Development of Magnesium-Lithium Base Alloys for Armor Plate. Report to Bureau of Aeronautics, Contract NOa(s) 9526, Battelle Memorial Institute (1950).
12. Busk, R. S., Leman, D. L. & Casey, J. J. The properties of some magnesium-lithium alloys containing aluminum and zinc. *JOM* **2**, 945–951 (1950).
13. Frost, P. D., Jackson, J. H., Loonam, A. C. & Lorig, C. H. The effect of sodium contamination on magnesium-lithium base alloys. *Trans. AIME* **188**, 1171–1172 (1950).
14. Frost, P. D., Kura, J. G. & Eastwood, L. W. Aging characteristics of magnesium-lithium base alloys. *JOM* **2**, 1277–1282 (1950).
15. Hibbard, W. R., Kearney, A. L., Hawley, W. H. & Burke, E. C. Solid solution alloys of magnesium with lithium and indium. *JOM* **3**, 978–979 (1951).
16. Freeth, W. E. & Raynor, G. V. The systems magnesium-lithium and magnesium-lithium-silver. *J. Inst. Metals* **82**, 575–580 (1953–54).
17. Rowland, J. A., Armantrout, C. E. & Walsh, D. F. Magnesium-rich corner of the magnesium-lithium-aluminum system. *JOM* **7**, 355–359 (1955).
18. Jones, W. R. D. & Hogg, G. V. The stability of mechanical properties of beta-phase magnesium-lithium alloys. *J. Inst. Met.* **85**, 255–261 (1956).
19. Clark, J. B. & Sturkey, L. The age hardening mechanism in magnesium-lithium-zinc alloys. *J. Inst. Met.* **86**, 272–276 (1957).
20. Payne, P. M. & Enyan, J. D. Note on the influence of sodium on magnesium-lithium alloys. *J. Inst. Met.* **86**, 351–352 (1957).
21. Bryer, T. G., Frost, P. D. & White, E. L. Final Technical Report on The Development of Magnesium-Lithium Alloys for Structural Applications. Report to National Aeronautics and Space Administration. Contract NAS8-5049. Battelle Memorial Institute (1963).
22. Drits, M. et al. *Magnesium-Lithium Alloys* [in Russian]. (Metallurgiya, Moscow, 1980).
23. Jackson, R. J. & Frost, P. D. Properties and Current Applications of Magnesium-Lithium Alloys. **NASA SP-5068** (1967).
24. Frost, P. D. Technical and Economic Status of Magnesium-Lithium Alloys. **NASA SP-5028** (1965).
25. Saia, A. High strength magnesium-lithium base alloys. **US Patent US119689A** (1964).
26. Wu, R. et al. Recent progress in magnesium–lithium alloys. *Int. Mater. Rev.* **60**, 65–100 (2014).
27. Sun, Y.-H., Wang, R.-C., Peng, C.-Q., Feng, Y. & Yang, M. Corrosion behavior and surface treatment of superlight Mg–Li alloys. *Trans. Nonferrous Met. Soc. China* **27**, 1455–1475 (2017).
28. Drits, M.E., Sviderskaya, Z.A., & Elkin, F.M. Effect of additional alloying on the structure and properties of β-phase magnesium-lithium alloys. *Russian Metallurgy (Metally)* **5**, 65–67 (1966).
29. Park, G. H. et al. Development of lightweight MgLiAl alloys with high specific strength. *J. Alloy. Compd.* **680**, 116–120 (2016).
30. Raynor, G. V. & Kench, J. R. The theta-phase in magnesium-lithium-silver alloys, with reference to instability after ageing. *J. Inst. Metals* **88** (1959–1960).
31. Rinnovatore, J. V. & Schwartz, M. The proposed structure of the transition phase and stability in Mg-Li-Al-Zn. *J. Inst. Met.* **92**, 188–189 (1964).
32. Tang, S. et al. Precipitation strengthening in an ultralight magnesium alloy. *Nat. Commun.* **10**, 1003 (2019).
33. Jackson, J. H. Magnesium-Lithium Base Alloys. United States patent (1956).
34. Rokhlin, L. L. The regularities in the Mg-rich parts of the phase diagrams, phase transformation and mechanical properties of Mg alloys with individual rare earth metals. *Arch. Metall. Mater.* **52**, 1–7 (2007).
35. Polmear, I. J. *Light Alloys*. 4th edn, (Butterworth-Heinemann, 2005).
36. Chakravorty, C. R. Development of ultra light magnesium-lithium alloys. *Bull. Mater. Sci.* **17**, 733–745 (1994).
37. Wang, S. J., Wu, G. Q., Li, R. H., Luo, G. X. & Huang, Z. Microstructures and mechanical properties of 5 wt.% Al_2Y_p/Mg–Li composite. *Mater. Lett.* **60**, 1863–1865 (2006).
38. Liu, B., Zhang, M. & Wu, R. Effects of Nd on microstructure and mechanical properties of as-cast LA141 alloys. *Mater. Sci. Eng.: A* **487**, 347–351, https://doi.org/10.1016/j.msea.2007.10.073 (2008).
39. Zhang, J. et al. Experimental study on strengthening of Mg–Li alloy by introducing long-period stacking ordered structure. *Scr. Materialia* **68**, 675–678 (2013).
40. Xu, T. C., Peng, X. D., Jiang, J. W., Zhang, X. & Wei, G. B. Microstructure and mechanical properties of Mg–Li–Al based alloy with yttrium addition. *Mater. Res. Innovations* **18**, S4-157-S154-162 (2014).
41. Xu, W. et al. A high-specific-strength and corrosion-resistant magnesium alloy. *Nat. Mater.* **14**, 1229–1235 (2015).
42. Kang, Z. X., Lin, K. & Zhang, J. Y. Characterisation of Mg–Li alloy processed by solution treatment and large strain rolling. *Mater. Sci. Technol.* **32**, 498–506 (2016).
43. Muga, C. O., Guo, H., Xu, S. S. & Zhang, Z. W. Effects of aging and fast-cooling on the mechanical properties of Mg-14Li-3Al-3Ce alloy. *Mater. Sci. Eng.: A* **689**, 195–202 (2017).
44. Li, R., Jiang, B., Chen, Z., Pan, F. & Gao, Z. Microstructure and mechanical properties of Mg14Li1Al0.3La alloys produced by two-pass extrusion. *J. Rare Earths* **35**, 1268–1272 (2017).
45. Zhang, M. et al. The effect of Y/Er and Zn addition on the microstructure and mechanical properties of Mg-11Li alloy. *Materials* **12**, 3066–3066 (2019).
46. Nordlien, J. H., Ono, S., Masuko, N. & NisancioĞlu, K. Morphology and structure of oxide films formed on magnesium by exposure to air and water. *J. Electrochem. Soc.* **142**, 3320–3322 (1995).
47. Taheri, M., Phillips, R. C., Kish, J. R. & Botton, G. A. Analysis of the surface film formed on Mg by exposure to water using a FIB cross-section and STEM–EDS. *Corros. Sci.* **59**, 222–228 (2012).
48. Makar, G. L. & Kruger, J. Corrosion of magnesium. *Int. Mater. Rev.* **38**, 138–153 (1993).
49. Esmaily, M. et al. Fundamentals and advances in magnesium alloy corrosion. *Prog. Mater. Sci.* **89**, 92–193 (2017).
50. Li, C. Q. et al. Composition and microstructure dependent corrosion behaviour of Mg-Li alloys. *Electrochim. Acta* **260**, 55–64 (2018).
51. Yan, Y. M. et al. Investigating the structure of the surface film on a corrosion resistant Mg-Li(-Al-Y-Zr) alloy. *Corrosion* **75**, 80–89 (2019).
52. Santucci, R. J., McMahon, M. E. & Scully, J. R. Utilization of chemical stability diagrams for improved understanding of electrochemical systems: evolution of solution chemistry towards equilibrium. *npj Mater. Degrad.* **2**, 1 (2018).
53. Hou, L. et al. Investigating the passivity and dissolution of a corrosion resistant Mg-33at.%Li alloy in aqueous chloride using online ICP-MS. *J. Electrochem. Soc.* **163**, C324–C329 (2016).
54. Haynes, W. M., Lide, D. R. & Bruno, T. J. *CRC Handbook of Chemistry and Physics*. (CRC Press, Boca Raton, FL, 2016).

55. Yan, Y., Qiu, Y., Gharbi, O., Birbilis, N. & Nakashima, P. N. H. Characterisation of Li in the surface film of a corrosion resistant Mg-Li(-Al-Y-Zr) alloy. *Appl. Surf. Sci.* **494**, 1066–1071 (2019).
56. Yan, Y. M. et al. On the in-situ aqueous stability of an Mg-Li-(Al-Y-Zr) alloy: role of Li. *Corrosion Sci.* 108342 (2019).
57. Yan, Y. et al. Investigating ion release using inline ICP during in situ scratch testing of an Mg-Li(-Al-Y-Zr) alloy. *Electrochem. Commun.* **99**, 46–50 (2019).
58. Matsuzawa, K., Koshihara, T., Ochiai, S. & Kojima, Y. The effect of additional element on the age-hardening characteristics and properties of Mg-Li alloys. *J. Jpn. Inst. Light Met.* **40**, 659–665 (1990).
59. Morishige, T. et al. Effect of Al composition on the corrosion resistance of Mg-14 mass% Li system alloy. *Mater. Transactions* **57**, 1853–1856 (2016).
60. Li, Y., Li, T., Wang, Q. & Zou, Y. in *Magnesium Technology 2019. The Minerals, Metals & Materials Series*. (eds Joshi, V. et al.) (Springer, Cham., 2019).
61. Lunder, O., Lein, J. E., Aune, T. K. & Nisancioglu, K. The role of Mg17Al12 phase in the corrosion of Mg alloy AZ91. *Corrosion* **45**, 741–748 (1989).
62. Kazakov, A. A., Timonova, M. A. & Borisova, L. G. Properties of magnesium-lithium alloys. *Met. Sci. Heat. Treat.* **25**, 682–684 (1983).
63. Zhang, C., Huang, X., Zhang, M., Gao, L. & Wu, R. Electrochemical characterization of the corrosion of a Mg–Li Alloy. *Mater. Lett.* **62**, 2177–2180 (2008).
64. Gao, L., Zhang, C., Zhang, M., Huang, X. & Sheng, N. The corrosion of a novel Mg–11Li–3Al–0.5RE alloy in alkaline NaCl solution. *J. Alloy. Compd.* **468**, 285–289 (2009).
65. Hanawalt, J. D., Nelson, C. E. & Peloubet, J. A. Corrosion studies of magnesium and its alloys. *Trans. AIME* **147**, 273 (1942).
66. McNulty, R. E. & Hanawalt, J. D. Some corrosion characteristics of high purity magnesium alloys. *J. Electrochem. Soc.* **81**, 423–433 (1942).
67. Boyer, J. A. The corrosion of magnesium and of the magnesium aluminum alloys containing manganese. *Am. Magnesium Corporation*, **248**, 417–454 (1927).
68. Payne, R. J. M. & Enyon, J. D. L. Discussion- The effect of sodium contamination on magnesium-lithium base alloys. *J. Inst. Met.* **191**, 557–558 (1951).
69. Kiszka, J. C. Stress corrosion tests of some wrought magnesium-lithium base alloys. *Mater. Prot.* **4**, 28–29 (1965).
70. Petty, R. L., Davidson, A. W. & Kleinberg, J. The anodic oxidation of magnesium metal: evidence for the existence of unipositive magnesium1,2. *J. Am. Chem. Soc.* **76**, 363–366 (1954).
71. Song, G., Atrens, A., John, D. S., Wu, X. & Nairn, J. The anodic dissolution of magnesium in chloride and sulphate solutions. *Corros. Sci.* **39**, 1981–2004 (1997).
72. Gomes, M. P. et al. On the corrosion mechanism of Mg investigated by electrochemical impedance spectroscopy. *Electrochim. Acta* **306**, 61–70 (2019).
73. Salleh, S. H., Thomas, S., Yuwono, J. A., Venkatesan, K. & Birbilis, N. Enhanced hydrogen evolution on Mg (OH)2 covered Mg surfaces. *Electrochim. Acta* **161**, 144–152 (2015).
74. Cain, T., Madden, S. B., Birbilis, N. & Scully, J. R. Evidence of the enrichment of transition metal elements on corroding magnesium surfaces using Rutherford backscattering spectrometry. *J. Electrochem. Soc.* **162**, C228–C237 (2015).
75. Taheri, M. et al. Towards a physical description for the origin of enhanced catalytic activity of corroding magnesium surfaces. *Electrochim. Acta* **116**, 396–403 (2014).
76. Hoche, D. et al. The effect of iron re-deposition on the corrosion of impurity-containing magnesium. *Phys. Chem. Chem. Phys.* **18**, 1279–1291 (2016).
77. Mercier, D., Swiatowska, J., Zanna, S., Seyeux, A. & Marcus, P. Role of segregated iron at grain boundaries on Mg corrosion. *J. Electrochem. Soc.* **165**, C42–C49 (2018).
78. Yuwono, J. A., Taylor, C. D., Frankel, G. S., Birbilis, N. & Fajardo, S. Understanding the enhanced rates of hydrogen evolution on dissolving magnesium. *Electrochem. Commun.* **104**, 106482 (2019).
79. Binns, W. J. et al. Physical and electrochemical evidence for the role of a Mg Hydride species in Mg alloy corrosion. *Corrosion* **75**, 58–68 (2019).
80. Hoey, G. R. & Cohen, M. Corrosion of anodically and cathodically polarized magnesium in aqueous media. *J. Electrochem. Soc.* **105**, 245–250 (1958).
81. Straumanis, M. E. & Bhatia, B. K. Disintegration of magnesium while dissolving anodically in neutral and acidic solutions. *J. Electrochem. Soc.* **110**, 357–360 (1963).
82. Samaniego, A., Birbilis, N., Xia, X. & Frankel, G. S. Hydrogen evolution during anodic polarization of mg alloyed with Li, Ca, or Fe. *Corrosion* **71**, 224–233 (2015).
83. Cain, T. W., Melia, M. A., Fitz-Gerald, J. M. & Scully, J. R. Evaluation of the potential range for sacrificial Mg anodes for the cathodic protection of Mg Alloy AZ31B-H24. *Corrosion* **73**, 544–562 (2017).
84. Glover, C. F., Cain, T. W. & Scully, J. R. Performance of Mg-Sn surface alloys for the sacrificial cathodic protection of Mg alloy AZ31B-H24. *Corros. Sci.* **149**, 195–206 (2019).
85. Birbilis, N., King, A. D., Thomas, S., Frankel, G. S. & Scully, J. R. Evidence for enhanced catalytic activity of magnesium arising from anodic dissolution. *Electrochim. Acta* **132**, 277–283 (2014).
86. Williams, G. & Neil McMurray, H. Localized corrosion of magnesium in chloride-containing electrolyte studied by a scanning vibrating electrode technique. *J. Electrochem. Soc.* **155**, C340 (2008).
87. Fajardo, S., Bosch, J. & Frankel, G. S. Anomalous hydrogen evolution on AZ31, AZ61 and AZ91 magnesium alloys in unbuffered sodium chloride solution. *Corros. Sci.* **146**, 163–171 (2019).
88. Cano, Z. P., McDermid, J. R. & Kish, J. R. Cathodic activity of corrosion filaments formed on Mg alloy AM30. *J. Electrochem. Soc.* **162**, C732–C740 (2015).
89. Cain, T. W., Glover, C. F. & Scully, J. R. The corrosion of solid solution Mg-Sn binary alloys in NaCl solutions. *Electrochim. Acta* **297**, 564–575 (2019).
90. Yuwono, J. A., Birbilis, N., Williams, K. S. & Medhekar, N. V. Electrochemical stability of magnesium surfaces in an aqueous environment. *J. Phys. Chem. C* **120**, 26922–26933 (2016).
91. Yuwono, J. A. et al. Aqueous electrochemistry of the magnesium surface: thermodynamic and kinetic profiles. *Corros. Sci.* **147**, 53–68 (2019).
92. Yang, Y., Scenini, F. & Curioni, M. A study on magnesium corrosion by real-time imaging and electrochemical methods: relationship between local processes and hydrogen evolution. *Electrochim. Acta* **198**, 174–184 (2016).
93. Lebouil, S., Gharbi, O., Volovitch, P. & Ogle, K. Mg dissolution in phosphate and chloride electrolytes: insight into the mechanism of the negative difference effect. *Corrosion* **71**, 234–241 (2015).
94. Cain, T. W., Gonzalez-Afanador, I., Birbilis, N. & Scully, J. R. The role of surface films and dissolution products on the negative difference effect for magnesium: comparison of Cl− versus Cl− free solutions. *J. Electrochem. Soc.* **164**, C300–C311 (2017).
95. Cano, Z. P. et al. Physical characterization of cathodically-activated corrosion filaments on magnesium alloy AZ31B. *Corrosion* **71**, 146–159 (2015).
96. Birbilis, N. et al. Nuclear microprobe analysis for determination of element enrichment following magnesium dissolution. *ECS Electrochem. Lett.* **4**, C34–C37 (2015).
97. Gore, P. et al. Enrichment efficiency of noble alloying elements on magnesium and effect on hydrogen evolution. *Corros. Sci.* **151**, 206–218 (2019).
98. Brady, M. P. et al. Film breakdown and nano-porous Mg(OH)2 formation from corrosion of magnesium alloys in salt solutions. *J. Electrochem. Soc.* **162**, C140–C149 (2015).
99. Unocic, K. A. et al. Transmission electron microscopy study of aqueous film formation and evolution on magnesium alloys. *J. Electrochem. Soc.* **161**, C302–C311 (2014).
100. Trasatti, S. Work function, electronegativity, and electrochemical behaviour of metals. *J. Electroanalytical Chem. Interfacial Electrochem.* **39**, 163–184 (1972).
101. Birbilis, N. et al. Poisoning the corrosion of magnesium. *Electrochem. Commun.* **34**, 295–298 (2013).
102. Liu, R. L. et al. Controlling the corrosion and cathodic activation of magnesium via microalloying additions of Ge. *Sci. Rep.* **6**, 28747 (2016).
103. Williams, G., Dafydd, H. A.-L., McMurray, H. N. & Birbilis, N. The influence of arsenic alloying on the localised corrosion behaviour of magnesium. *Electrochim. Acta* **219**, 401–411 (2016).
104. Yuwono, J. A. et al. Aqueous electrochemical activity of the Mg surface: the role of group 14 and 15 microalloying elements. *J. Electrochem. Soc.* **164**, C918–C929 (2017).
105. Liu, R. L., Scully, J. R., Williams, G. & Birbilis, N. Reducing the corrosion rate of magnesium via microalloying additions of group 14 and 15 elements. *Electrochim. Acta* **260**, 184–195 (2018).
106. Liu, R. L., Zeng, Z. R., Scully, J. R., Williams, G. & Birbilis, N. Simultaneously improving the corrosion resistance and strength of magnesium via low levels of Zn and Ge additions. *Corros. Sci.* **140**, 18–29 (2018).
107. Jiang, P. et al. Microstructural influence on corrosion behavior of MgZnGe alloy in NaCl solution. *J. Alloy. Compd.* **783**, 179–192 (2019).
108. Limmer, K. R., Williams, K. S., Labukas, J. P. & Andzelm, J. W. First principles modeling of cathodic reaction thermodynamics in dilute magnesium alloys. *Corrosion* **73**, 506–517 (2017).
109. Cain, T.W. & Labukas, J.P. in *Magnesium Technology 2020. The Minerals, Metals & Materials Series*. (eds Jordon, J. et al.) (Springer, Cham., 2020).

AUTHOR CONTRIBUTIONS

Both T.W.C. and J.P.L. contributed equally to the literature survey, writing, and editing of this work.

COMPETING INTERESTS

The authors declare no competing interests.

ADDITIONAL INFORMATION

Supplementary information is available for this paper at https://doi.org/10.1038/s41529-020-0121-2.

Correspondence and requests for materials should be addressed to T.W.C.

Reprints and permission information is available at http://www.nature.com/reprints

Publisher's note Springer Nature remains neutral with regard to jurisdictional claims in published maps and institutional affiliations.